[CANCER RESEARCH 46, 5320–5329, October 1986]

Oxygenation and Differentiation in Multicellular Spheroids of Human Colon Carcinoma[1]

R. M. Sutherland,[2] B. Sordat, J. Bamat, H. Gabbert, B. Bourrat, and W. Mueller-Klieser

University of Rochester Cancer Center and Departments of Radiation Biology and Biophysics and of Radiation Oncology, Rochester, New York [R. M. S.]; Swiss Institute for Experimental Cancer Research, 1066 Epalinges, Switzerland [B. S., J. B.]; and Departments of Pathology [H. G.] and of Applied Physiology [B. B., W. M-K.], University of Mainz, D-6500 Mainz, Federal Republic of Germany

ABSTRACT

Oxygenation and development of necrosis were evaluated in multicellular spheroids of poorly differentiated (HT29) and moderately well-differentiated (Co112) human adenocarcinoma of the colon. Spheroids were grown *in vitro* under well-controlled oxygen and nutrient conditions in spinner flasks up to sizes of 2800-μm diameter after 5 wk of culture. Morphological studies showed that the Co112 spheroids contained pseudoglandular structures with lumen, very similar to the characteristics of the original tumor specimen from the patient and to the cells when grown as xenograft tumors in nude mice. Microelectrodes were used to measure the oxygen tension (PO_2) profile within individual spheroids at different stages of growth. Histological sections through the centers of spheroids were measured to determine the thickness of the viable rim of cells surrounding spheroid necrotic centers in order to estimate the size of the severely hypoxic zone of cells by comparison with the PO_2 profiles of the same spheroids. The data demonstrate significant differences between these two human colon tumor spheroid systems. Both spheroid types exhibited steep PO_2 gradients at relatively small sizes of <600-μm diameter, but for any given size in this range, the more differentiated Co112 spheroids were more hypoxic. Although severe hypoxia (PO_2, <10 mm of Hg) was present in both spheroid types at larger sizes, there was a significant difference in the central PO_2 values which were between 5 and 10 mm of Hg in large Co112 spheroids but remained at or close to 0 mm of Hg in large HT29 poorly differentiated human colon tumor spheroids. The presence of pseudoglandular structures and lumen in the Co112 spheroids was associated with changes in the shape of PO_2 profiles. Such profiles have not previously been seen in other poorly differentiated human or rodent tumor spheroids. Furthermore, the PO_2 profiles of both of these human tumor spheroid types were often continuously curving with a very shallow gradient in the inner edge of the viable rim of cells surrounding the necrotic center. Regulation of oxygen consumption and/or diffusion in these inner regions of human spheroids could produce these continuously curving PO_2 gradients.

INTRODUCTION

The efficiency of oxygenation of tumor microregions may be severely compromised due to poor and/or abnormal development of a vascular network as well as altered supply and consumption of metabolites. Although there has been direct and indirect evidence in experimental tumor systems for severe hypoxia, such evidence has been limited for human tumor systems. However, responses of some human tumors to radiation therapy have been shown by indirect methods to be affected by altering the oxygen supply from the blood (1, 2). More direct evidence of poor oxygen supply in human tumors has been obtained using oxygen microelectrodes (3) and using cryospectrophotometric measurements of tumor biopsies (4, 5). In the latter case, significant heterogeneity of oxyhemoglobin levels in microvessels among and within tumor biopsies of well-differentiated rectal adenocarcinomas, as well as squamous cell carcinomas of the head and neck, was found.

In addition to the presence of gradients of oxygen concentration, gradients of other metabolites and catabolites are likely to occur. The concentrations of these substances may decrease with distance from microvessels as in the case of oxygen or may increase as for lactate. Thus, tumor cells are exposed to a wide range of microenvironments, which may significantly affect their phenotypic expression for malignant properties and therapeutic responses. It is well known that hypoxia can increase radiation resistance, and it has been shown that drug responses may also be affected (6–8).

Tumor microregions often develop areas of hypoxia and acidosis as well as deprivation of critical nutrients such as glucose. These regions may be associated with neighboring areas of necrosis and toxic products. To model the effects of three-dimensional growth and chronic development of these heterogeneous microenvironments at different stages of growth of tumor microregions, the multicell spheroid *in vitro* tumor model was used in the experiments described in this paper (9–11). Significant cellular and microenvironmental heterogeneities and development of quiescent cell populations have previously been demonstrated in spheroids of rodent tumor systems (12–16).

Three-dimensional growth of cells in spheroids facilitates direct and close range cell-cell interactions which may modify the cellular metabolism and thus responses to therapeutic agents (17–21). It was shown using V79 hamster lung and EMT6 mouse mammary cells that oxygen consumption per cell or per volume of viable spheroid "tissue" decreased approximately 3-fold with increase in size in the range of 200- to 600-μm diameter, apparently partly in association with the development of quiescent populations of cells (22–24). In addition to this effect on oxygen consumption, we have also recently demonstrated the importance of nutrients such as glucose (25) for the respiratory activity and regulation of necrosis development of spheroids.

Close cell-cell interactions and tissue-like three-dimensional structure are often necessary prerequisites for differentiation which has been observed in some spheroids of embryonic and adult normal and tumor cells (26–28). Spheroids have also been shown to develop extracellular matrix material which may modulate differentiation (29, 30). In this paper we have studied spheroids of two human adenocarcinomas of colon which are poorly and moderately differentiated. Limited data on spheroids of carcinomas such as colon, especially as related to differentiation state, are available. We have recently developed a moderately differentiated colon carcinoma spheroid system, which exhibits marked similarity of growth and morphological characteristics to tumors *in vivo*, both to the original tumor from the patient and to tumor xenografts in nude mice. It was of interest to compare the oxygenation within these differentiating human tumor spheroids as measured by microelectrodes

Received 7/23/85; revised 4/22/86, 6/16/86; accepted 6/20/86.

The costs of publication of this article were defrayed in part by the payment of page charges. This article must therefore be hereby marked *advertisement* in accordance with 18 U.S.C. Section 1734 solely to indicate this fact.

[1] This research was supported by NIH Grants CA 11051, CA 11198, and CA 20329; by Grants MU576/1 and MU576/2-1 from the Deutsche Forschungsgemeinschaft; and by the Swiss Institute for Experimental Cancer Research, Lausanne, Switzerland.

[2] Supported by the Alexander von Humboldt Foundation by a Senior United States Scientist Award during part of the period during which this research was performed. To whom requests for reprints should be addressed.

with data obtained previously on poorly differentiated rodent tumor spheroids to determine possible differences in regulation of oxygen metabolism. The relationship of the development of necrosis to the oxygenation within the spheroids was also studied using histological techniques.

MATERIALS AND METHODS

Cell Lines and Spheroid Culturing. The HT29 cell line of colon adenocarcinoma was originally established as a xenograft by Fogh (31) and was supplied to us by him. The cells used in these experiments were in passages 170 to 173. HT29 cells have previously been grown as spheroids by us and others (32, 33). The Co112 line was established *in vitro* from a xenograft of human tumor in nude mice (34) and was in passages 48 to 53 during the experiments. They had not previously been characterized for growth as spheroids.

Both cell lines were maintained in DMEM[3] (25 mM glucose) supplemented with 10% fetal bovine serum. Spheroid growth was initiated from cells in the exponential growth phase by inoculating 5×10^5 cells in 10 ml of medium into microbiological Petri dishes (100 mm). Five days after initiation of spheroid growth, the cell aggregates were transferred into spinner flasks (150 rpm) containing 100 ml of DMEM medium plus 10% serum equilibrated with 5% CO_2 (v/v) and air. The medium was replenished on alternate days as the spheroids grew up to about 500 μm, and daily thereafter. The number of spheroids was reduced as they grew in order to maintain a relatively constant cell/medium ratio and, therefore, a sufficient nutrient and oxygen supply (35). When spheroids reached diameters greater than about 1500 μm, the flasks contained no more than about 100 spheroids/100 ml of medium.

Oxygen Microelectrode Measurements. The PO_2 values in the spheroids were determined under conditions which attempted to match those to which the spheroids were exposed during growth (36). The PO_2 electrode was inserted by micromanipulation into a spheroid in stirred medium, and values were recorded on radial tracks through the center of the spheroids. Additional details of methodological aspects of microelectrode measurements as well as calibration and performance have been published elsewhere (14, 15, 37).

Histology. Serial sections of 2-μm thickness were made of spheroids and tumors fixed in 2.5% glutaraldehyde and embedded in JB-4 plastic (Polysciences, Inc., Warrington, PA). The sections were stained with Giemsa. Some histological investigations were also carried out using standard paraffin sections stained with hematoxylin-eosin. The thickness of the viable rim of cells surrounding the necrotic centers was determined from central sections using a microscope micrometer. By comparing spheroid sizes before and after fixing and sectioning, the shrinkage caused by the histological procedures was determined for individual spheroids. This ranged from 8 to 25%, and all measurements were corrected for this shrinkage.

For electron microscopy the specimens were fixed with 2.5% glutaraldehyde in cacodylate buffer, washed, postfixed in 1% osmium tetroxide, and embedded in araldite.

RESULTS

Morphology and Differentiation Characteristics. The histological characteristics of the human colon multicellular tumor spheroids studied in these experiments are presented in Fig. 1 for HT29 cells and in Fig. 2 for Co112 cells. The HT29 spheroids grew at a rate of about 30-μm-diameter increase/day, which was about 30% faster than the growth rate of the Co112 spheroids. When the spheroids attained diameters of approximately 450 to 500 μm, histological sections through the centers demonstrated that central necrotic regions had begun to form. Large spheroids exhibited viable rims of cells of approximately 200-μm thickness surrounding large necrotic centers. The spheroids were grown for up to 5 wk so that a wide range of diameters, between approximately 200 μm and 2800 μm, was available for measurement of oxygenation using microelectrodes.

The Co112 spheroids exhibited morphological evidence of colonic tumor cell differentiation (Fig. 3). Glandular-like structures consisting of lumen surrounded by closely apposed cells with basally oriented pleomorphic nuclei were present. At the electron microscopic level, microvillous projections extending on the lumenal side and a variety of junctional complexes including desmosomes could be found. The cytoplasm contained Golgi structures, cytokeratin-like filaments, and some secretory granules in apical regions. These ultrastructural features of the Co112 spheroids, as illustrated in Fig. 3, *D*, *E*, and *inset*, are essentially identical to those present when these human tumor cells are grown as xenografts in nude mice. As represented in Fig. 3*A*, the original patient tumor from which the s.c. passaged xenograft as well as the *in vitro* established cell line were then derived was a moderate differentiated adenocarcinoma, Dukes' Class C. These characteristics were maintained in solid grafts following tumor cell inoculation s.c. or within the wall of the nude mouse large bowel (38). As illustrated in Fig. 3, *B* and *C*, multi- or uninodular tumor masses can be seen infiltrating the smooth muscle cell layers or expansively growing as spheroid-like structures *in vivo* within the mesentery of the mouse. Using immunocytochemical techniques, both Co112 spheroids and xenografts were shown to express CEA associated with the apical lining of the tumor cells forming glandular-like structures (Ref. 39; Footnote 4). Within deeper hypoxic regions of Co112 spheroids, CEA reactivity appeared as intracellular deposits which were more pronounced than in cortical areas. Unlike the Co112 spheroids, HT29 cells formed poorly differentiated spheroids as well as xenografts in the nude mouse which very occasionally contained acinar structures. Thus, the two spheroid systems used in this investigation exhibit considerably different growth and morphological properties.

Oxygenation Measurements. PO_2 microelectrode measurements through the centers of individual spheroids were obtained as shown in Fig. 4. The PO_2 decreased in the medium outside the spheroid as the microelectrode was advanced by the micromanipulator towards the spheroid surface. This is due to an unstirred diffusion-depleted zone associated with the high local O_2 consumption by the spheroid. The PO_2 gradient in this zone outside the spheroid can be used to calculate the O_2 consumption rate within the viable rim of spheroid cells under certain conditions (37). The microelectrode is advanced from the spheroid surface into the viable rim of cells for different incremental distances and stopped for about 30 s to obtain steady-state PO_2 values. At or near the transition zone between the viable rim of cells and the necrotic center, there is no further decrease in PO_2. The PO_2 in this plateau region is often at or close to 0 mm of Hg for large spheroids but can be considerably greater depending on the external O_2 and glucose supply (25). Small spheroids (<500 μm) may not exhibit a plateau but rather a hyperbolic PO_2 profile with a nadir in the spheroid center. Fig. 5, *A* and *B*, illustrates the same data as Fig. 4 for which the individual steady-state PO_2 values are plotted *versus* the distance into the spheroid. This is superimposed over the histolog-

[3] The abbreviations used are: DMEM, Dulbecco's modified Eagle's medium; PO_2, oxygen tension; CEA, carcinoembryonic antigen; BME, Eagle's basal medium.

[4] R. Sutherland, F. Buchegger, M. Schreyer, A. Vacca, and J-P. Mach. Penetration and binding of radiolabeled anti-CEA monoclonal antibodies and their $F(AB')_2$ and Fab fragments in human colon multicellular tumor spheroids, submitted for publication.

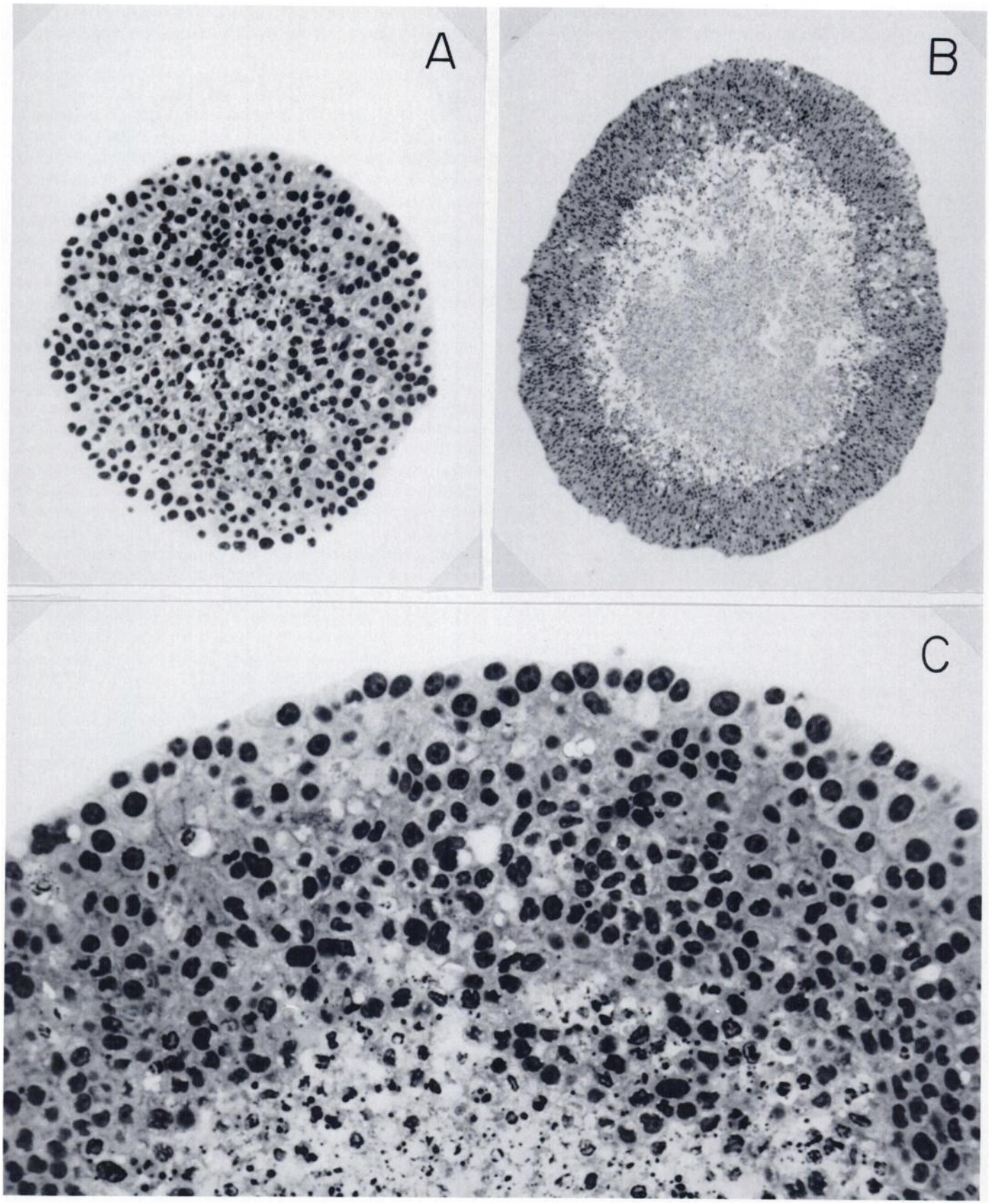

Fig. 1. Histology of poorly differentiated human colon adenocarcinoma HT29 cell spheroids. *A*, central section of small spheroid of 380-μm diameter before development of central necrosis. × 125. *B*, central section of spheroid of 1415-μm diameter after 18 days in culture demonstrating viable rim of cells surrounding an extensive necrotic center. × 60. *C*, high magnification (× 310) showing structural arrangement of spheroid cells in the viable rim of approximately 225-μm thickness.

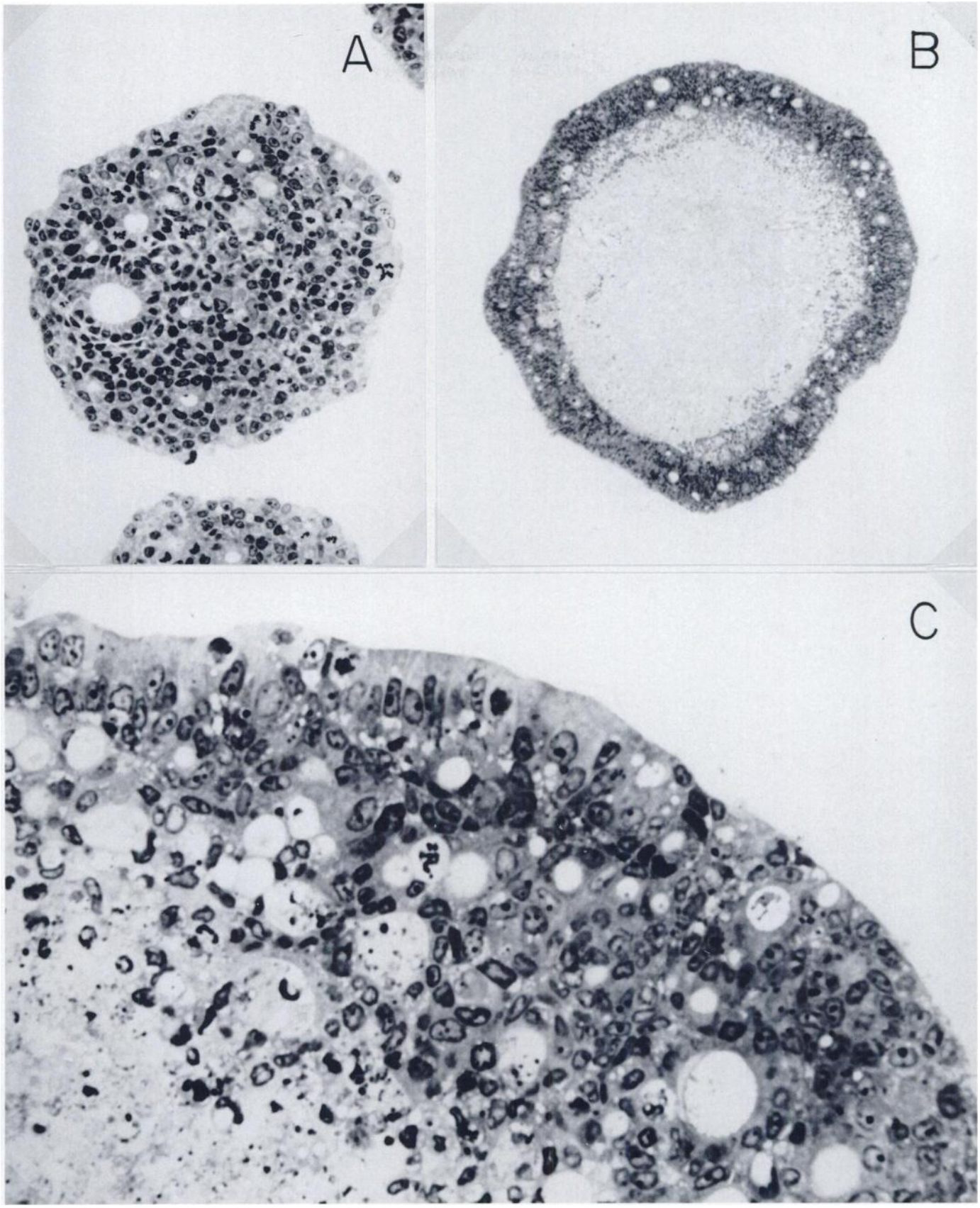

Fig. 2. Histology of moderately well-differentiated human colon adenocarcinoma Co112 cell spheroids. *A*, central section of small spheroid of 355-μm diameter before development of central necrosis. These spheroids contain many differentiated pseudoglandular structures with lumen and express CEA. × 125. *B*, central section of spheroid of 1480-μm diameter after 24 days in culture demonstrating the viable rim of cells containing acini surrounding an extensive necrotic center. × 60. *C*, high magnification (× 310) showing structural arrangements of spheroid cells and pseudoglandular structures in the viable rim of approximately 185-μm thickness.

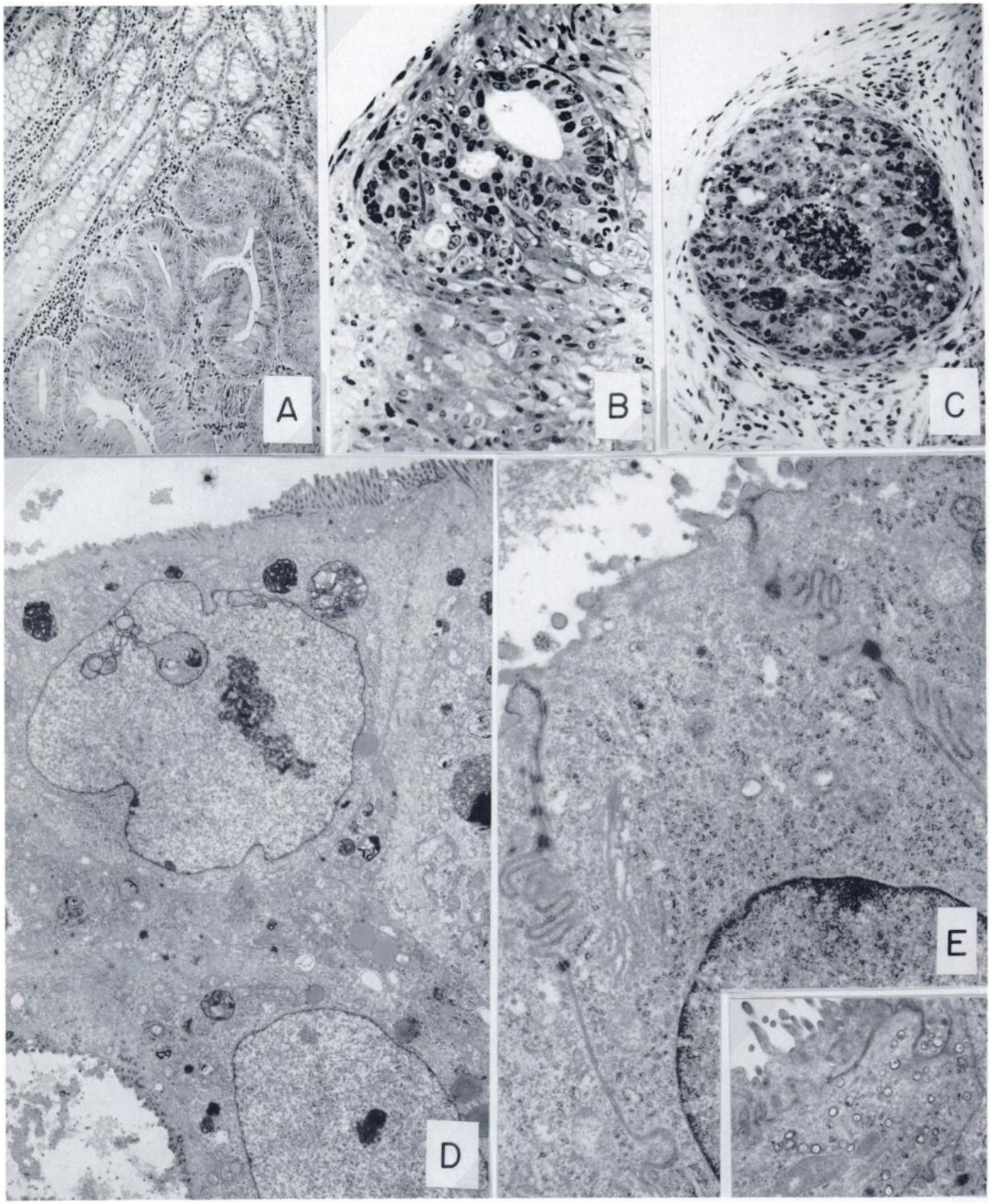

Fig. 3. *A*, original Co112 patient tumor forming pseudoglandular tumor cell cords with some mucin production. Classified as a moderately differentiated sigmoid adenocarcinoma, it is shown here at the invasion front adjacent to normal sigmoid crypts. H&E, × 375. *B*, Co112 tumor cells developing as an invasive focus within smooth muscle cell layers of the large bowel following *in situ* implantation in the nude mouse. Note preservation of the pseudoglandular structures. Giemsa staining on plastic-embedded tissue sectioned at 2 μm, × 375. *C*, Co112 tumor nodule growing *in vivo* into the mesentery of a nude mouse following gut implantation of tumor cells. The nodule has a central necrotic core evoking a spheroid organization, and pseudoglands filled with dense material are preserved. Giemsa, × 930. *D*, external border region of a Co112 spheroid grown *in vitro* and displaying several carcinoma cells with epithelial characteristics; part of an intercellular lumen can be seen in the *lower left corner*. × 7,000. *E*, detailed view of a Co112 carcinoma cell lining a pseudoglandular structure within a spheroid. Tight-like junctions, desmosomes, and intercellular membrane identations indicate the maintenance of a degree of epithelial cell polarity. × 17,500. *Inset*, apical regions containing occasionally secretory-like granules. × 9,200.

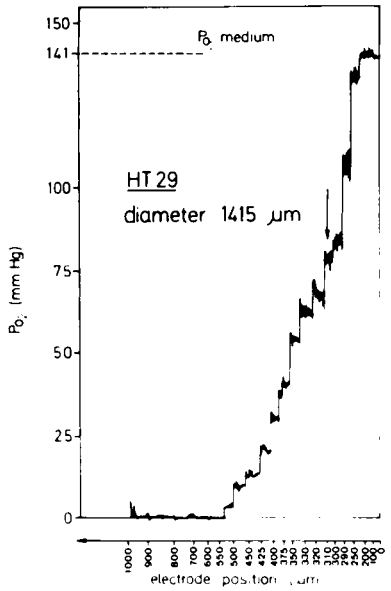

Fig. 4. PO_2 microelectrode profile recording for a 1415-μm-diameter HT29 human colon adenocarcinoma spheroid. ↓, surface of the spheroid. The microelectrode was advanced at different incremental distances into the spheroid and stopped at each location to obtain steady-state PO_2 values. This recording illustrates typical data for spheroids demonstrating a diffusion-depleted zone with reduced PO_2 surrounding the spheroid, a gradient within the viable rim, and a plateau associated with the necrotic center and sometimes with the inner cell layers of the histologically viable rim of cells.

ical section of the same spheroid from which the PO_2 profile was obtained to indicate the relation of the profile to the structure.

Representative PO_2 profiles from different HT29 spheroids of a wide range of sizes are presented in Fig. 6. It can be seen that a major shift of the profiles occurs in the direction of increased hypoxia over a relatively small size range between approximately 400- and 1000-μm diameter, compared to the change in the profile between approximately 1000 and 2300 μm. In general, the diffusion-depleted zone is more extended in large spheroids than in small ones. Many of the PO_2 profiles recorded in these spheroids exhibit a steep initial PO_2 gradient close to the spheroid surface and a more shallow PO_2 gradient in the inner part of the spheroid; *e.g.*, small spheroids (≤400 μm) often show PO_2 distributions that are not parabolic, a result which is different from previous findings in spheroids of rodent cells (14, 15) and which is indicative of a nonuniform O_2 consumption rate and/or diffusion constant in these spheroids (37). The central PO_2 values are far above 0 mm of Hg in the size range of 300 to 700 μm. The PO_2 in the center decreases as the spheroid increases in diameter; severe hypoxia, *i.e.*, PO_2 values close to 0 mm of Hg, was present in spheroids with diameters larger than 700 μm.

Similar data were obtained for the Co112 spheroids but with some major differences (Fig. 7). Unlike the HT29 spheroids, the PO_2 values measured within many of these spheroids exhibited distinct changes in the rate of decline as the microelectrode was advanced toward the center. These changes in the PO_2 profiles appear to be due to the pseudoglandular structures in these spheroids, since such profiles have never been observed by us for many other types of spheroids not containing these differentiated structures. Another significant difference found in the Co112 spheroids compared with the HT29 spheroids is the tendency for the central PO_2 to increase to an average value of 5 mm of Hg (range, between 0 and 10 mm of Hg) for spheroids larger than about 1000-μm diameter (Fig. 7*C*). On the other hand, almost all spheroids in the range of 600 to 1000 μm exhibited a central PO_2 of 0 mm of Hg (Fig. 7*B*). It should also be noted that, similar to the HT29 spheroids, the Co112 spheroids often exhibited profiles with a relatively steep initial slope which continuously became more shallow, so that the slope associated with the inner region of the viable rim of cells was sometimes very shallow and extended in length (Fig. 7*C*).

Fig. 8 presents the data for the central PO_2 measurements for all spheroids for which complete PO_2 profiles were obtained. When these central PO_2 values are plotted *versus* the diameter of the spheroid from which they were measured, it can be seen that the central PO_2 declines rapidly over the size range of 300 to 700 μm for HT29 spheroids, but it declines even more steeply and over a smaller size range (200 to 500 μm) for Co112 spheroids. Much lower central PO_2 values are found in Co112 spheroids compared to HT29 for similar sizes in this range; for example, the central PO_2 in 450-μm Co112 spheroids is close to 0 mm of Hg but is approximately 30 mm of Hg in HT29 spheroids. While the central PO_2 remained at 0 mm of Hg for almost all HT29 spheroids greater than 700-μm diameter, the central PO_2 values of the Co112 spheroids greater than 1000 μm showed the opposite tendency; that is, they were almost all increased to between 5 and 10 mm of Hg.

It was also possible to assess the histologically viable rim thickness of indvidual spheroids for which complete PO_2 profiles had been determined. By comparing the distance into the spheroid at which the severely hypoxic plateau of PO_2 begins with the histological rim thickness, an estimate of the thickness of the severely hypoxic cell layers surrounding the necrotic centers can be obtained. For the size range of spheroids examined, the severly hypoxic central plateau of the PO_2 profiles occurred at 0 mm of Hg for HT29 spheroids and at an average PO_2 of 5 mm of Hg (range, 0 to 10 mm of Hg) for Co112. Table 1 presents this analysis for those spheroids for which both suitable histology and profiles were available. The histological rim thickness extended into the Co112 spheroids an average of 44 μm beyond the distance where the severely hypoxic PO_2 plateau began, and 47 μm beyond the point where the PO_2 plateau began in the HT29 spheroids. Of a total of 21 such determinations for both spheroid types, 19 indicated that this zone of severely hypoxic but histologically intact cells was present. However, only a small portion of viable cells was located within the severely hypoxic region in many of the very large spheroids; for example, the 5 HT29 spheroids with the thinnest hypoxic rims (see Table 1) averaging only 11 μm had an average diameter of 1930 μm. On the other hand, the 6 spheroids with the histological rims extending an average of 68 μm into the hypoxic plateau were smaller, with a mean diameter of 1424 μm. Similarly, the 4 largest Co112 spheroids with the thinnest histological rim extending within the severely hypoxic plateau averaging only 3 μm were 2298-μm mean diameter, but the 7 other spheroids of smaller mean diameter of 1584 μm exhibited a histological rim of an average thickness of 75 μm extending within the severely hypoxic central plateau region.

This type of analysis was also extended to include all of the measurements (not just to matched pairs of data as in Table 1) of histological rim thickness and of distance into the spheroids where the severely hypoxic plateau begins. The additional spheroids from which measurements of histological rim thickness were obtained were from the same population as those for which PO_2 profiles were determined. Similar results to those presented in Table 1 were obtained. For both spheroid types the histological rim thickness was greater than the distance into the spheroid where the severely hypoxic plateau begins. This

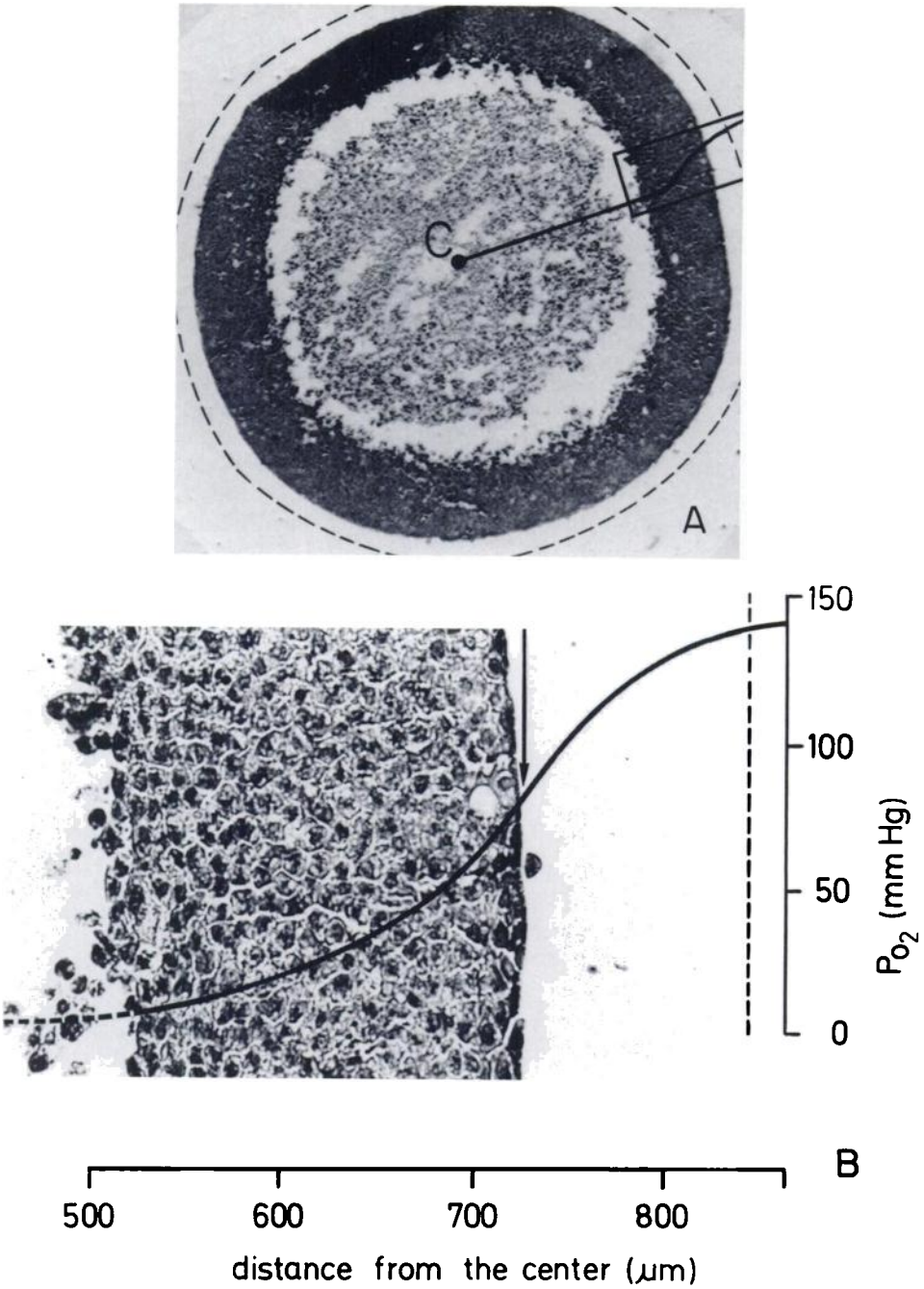

Fig. 5. Same data as in Fig. 4, but the individual steady-state PO_2 values are used to obtain a curve of PO_2 *versus* distance into the spheroid. This PO_2 profile is shown superimposed over the histological section of the same spheroid structure (*A*) and to a magnified section of the viable rim (*B*). The *dashed line* indicates the edge of the diffusion-depleted zone where the PO_2 just begins to decline as the electrode approaches the spheroid. The geometric center of the spheroid is designated as *C*. *A*, × 78; *B*, × 420.

was an average of 30 μm for Co112 (191 μm minus 161 μm) and 25 μm for HT29 (216 μm minus 191 μm) (Table 2).

DISCUSSION

The data obtained in these experiments have demonstrated the development of severe hypoxia and steep PO_2 gradients within spheroids of human colon adenocarcinoma at relatively small sizes, in the range of less than 600-μm diameter. Both the poorly differentiated HT29 and moderately differentiated Co112 spheroids exhibited severe hypoxia at diameters greater than 600 to 700 μm, but the incidence of severe hypoxia was higher in Co112 than in HT29 spheroids for this size range. The central PO_2 values for both spheroid types decreased rapidly as spheroid diameter increased between 200 and 600 μm. For any given size of spheroid in this range, the Co112 spheroid exhibited greater hypoxia. We have previously reported marked decreases of central PO_2 values *versus* spheroid size over similar ranges of PO_2 values and spheroid sizes for hamster V79 lung cell spheroids and for mouse EMT6 mammary tumor spheroids grown in BME in high glucose (16.5 mM) which is similar to the high glucose level present in the medium used in the present experiments (25 mM DMEM). A more shallow decline of central PO_2 values with increasing spheroid size was registered in EMT6 spheroids cultured in BME with 5.5 mM glucose (15, 25). These findings indicate that the development of hypoxic

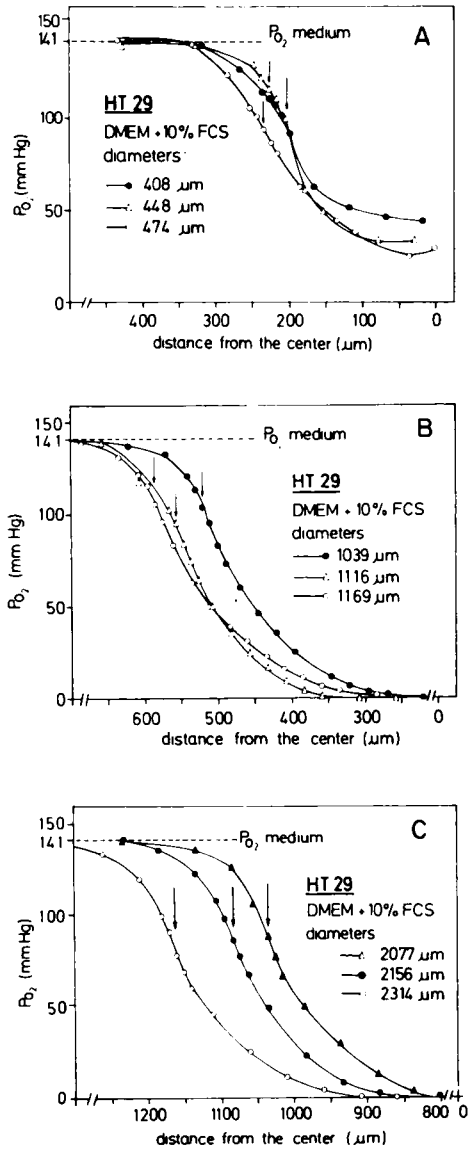

Fig. 6. PO_2 microelectrode profiles of HT29 spheroids of different ranges of diameter: 400 to 500 µm (*A*); 1000 to 1200 µm (*B*); >2000 µm (*C*). The *arrows* indicate the surfaces of the spheroids. *FCS*, fetal calf serum.

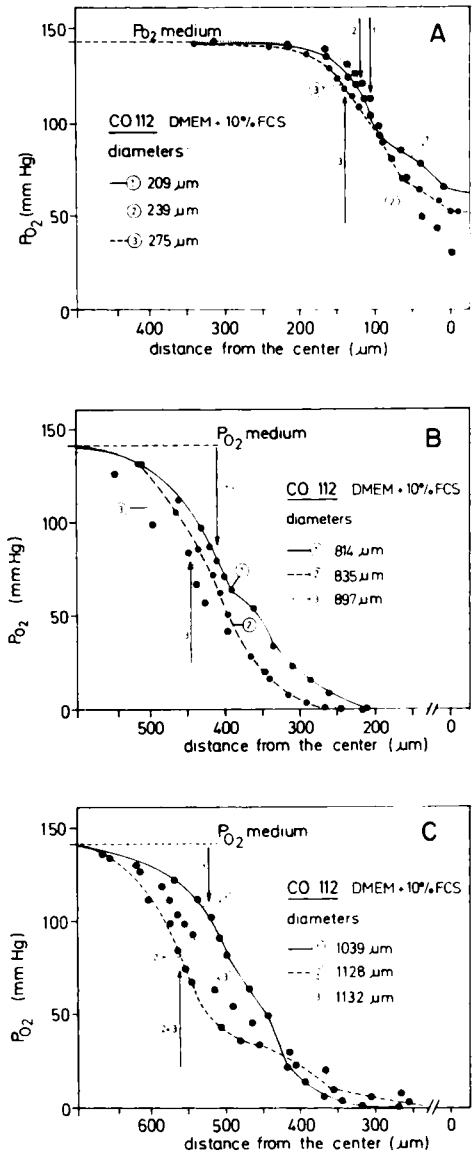

Fig. 7. PO_2 microelectrode profiles of Co112 spheroids of different ranges of diameter: 200 to 300 µm (*A*); 800 to 900 µm (*B*); 1000 to 1200 µm (*C*). The *arrows* indicate the surfaces of the spheroids. *FCS*, fetal calf serum.

regions of viable cells in spheroids may be influenced by the inherent properties of the cell line and by factors in the culture medium, such as the concentration of glucose.

For spheroids of larger diameters with extensive central necrotic regions, there were other significant differences in the PO_2 profiles and in central PO_2 values measured when comparing the poorly differentiated (HT29) and the more differentiated (Co112) human tumor spheroids with each other and to previous experiments with rodent spheroids. There was a significant difference in the central PO_2 values which were between 5 and 10 mm of Hg in large Co112 spheroids but remained at or close to 0 mm of Hg in large HT29 poorly differentiated human colon spheroids. Also, Co112 spheroids exhibited significant structure in the PO_2 profiles, probably associated with the pseudoglands and the differentiation grade. Furthermore, there was a continuous decrease in the slope of the PO_2 profiles of many of the spheroids of both Co112 and HT29 cell lines; an initial steep slope often became a more shallow gradient in the inner zone of cells surrounding the necrotic center. This was not observed previously in V79 or EMT6 spheroids using the same spheroid growth and PO_2 measuring procedures as those

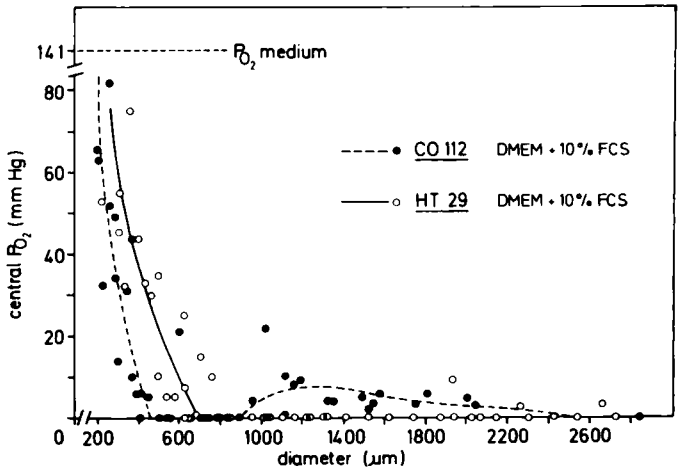

Fig. 8. Central PO_2 values of Co112 and HT29 spheroids of different diameters. Each *point* is from an individual spheroid. *FCS*, fetal calf serum.

Table 1 *Comparison of thickness of rim of cells surrounding the necrotic centers of spheroids as determined histologically and from PO_2 microelectrode profiles*

	Spheroid diameter (μm)	Rim thickness (μm)		Hypoxic rim thickness (μm)
		Histology[a]	Microelectrode[b]	Histology-microelectrode
Co112	1035	211	160	51
	1203	193	150	43
	1335	244	110	134
	1360	210	160	50
	1504	228	140	88
	1532	208	125	83
	2011	156	200	−44
	2051	179	150	29
	2857	177	200	−23
	2271	176	150	26
	1716 ± 566[c]	198 ± 27	155 ± 29	44 ± 52
HT29	1026	257	160	97
	1039	248	186	62
	1310	237	150	87
	1324	189	250	39
	1415	196	174	22
	1532	203	200	3
	1631	215	150	65
	1751	235	180	55
	1887	226	155	71
	2035	266	250	16
	2739	203	199	4
	1608 ± 494	225 ± 26	178 ± 31	47 ± 33

[a] Measured on histological sections through centers of spheroids as in Figs. 1 and 2.
[b] Measured as the distance from where the electrode enters the spheroid to where the PO_2 profile begins to plateau as in Fig. 4.
[c] Mean ± SD.

Table 2 *Measurements of thickness of spheroid viable rims*

Rim thickness (μm)	Co112	HT29
Histology[a]	191 ± 30[b] (14)[c]	216 ± 43 (17)
PO_2 microelectrode[d]	162 ± 39 (28)	191 ± 36 (17)

[a] Measured on histological sections through centers of spheroids as in Figs. 1 and 2.
[b] Mean ± SD.
[c] Numbers in parentheses, number sized.
[d] Measured as the distance from where the electrode enters the spheroid to where the PO_2 profile begins to plateau as in Fig. 4.

used in the experiments reported here. However, Carlsson *et al.* (16, 40) have previously reported gradual decreases in the steepness of PO_2 profiles for both rodent and human spheroids grown in liquid overlay culture and measured with microelectrodes after attachment of the spheroids to coverslips. Continuously bending PO_2 profiles may thus be a characteristic of the particular cell line used for spheroid growth and may not necessarily be specific for spheroids from human cells.

By comparing the histological rim thickness to the thickness of the viable rim as determined by the change in the PO_2 gradient to a plateau in the center, it was possible to estimate the potential for a fraction of radiation-resistant hypoxic cells (PO_2, <10 mm of Hg) within the histologically intact viable rim. The data indicate the presence of a cell zone of at least 25- and perhaps up to 50-μm thickness which would be severely hypoxic, although there is considerable uncertainty in this estimate, since it was determined by the difference of two values, each with significant potential errors of measurements. However, no experiments have been done to determine whether there are clonogenic cells within this fraction for these two spheroid cell lines. A significant fraction of clonogenic cells has been reported in this region for other types of spheroids (12, 13). Interestingly, in large spheroids with large necrotic centers there were very few histologically intact cells within the severely hypoxic compartment. This suggests that the geometry is less favorable for diffusion in such large spheroids as has been suggested theoretically (37) and/or that necrotic material may have toxic effects and reduce the size of this compartment. Direct cytostatic and cytotoxic effects from products of spheroid necrosis have recently been demonstrated by Freyer (41).

The data in these experiments suggest that cell differentiation can cause differences in tissue oxygenation within tumor microregions, possibly associated with local differences, such as the pseudoglandular structures in these colon spheroids, but also possibly due to metabolic differences in differentiated cells associated with consumption of oxygen and other nutrients. Furthermore, the data presented here show that at least some human tumor spheroids may exhibit continuously bending PO_2 profiles which may be indicative of nonuniform O_2 consumption rates and/or O_2 diffusion properties in these spheroids.

ACKNOWLEDGMENTS

Technical assistance provided by D. Piquet is gratefully acknowledged.

REFERENCES

1. Bush, R. S., Jenkin, R. D. T., Allt, W. E. C., Beale, F. A., Bean, H., Dembo, A. J., and Pringle, J. F. Definitive evidence for hypoxic cells influencing cure in cancer therapy. Br. J. Cancer, *37* (Suppl. 3): 302–306, 1978.
2. Dische, S., Anderson, P. J., Sealy, R., and Watson, E. R. Carcinoma of the cervix—anaemia, radiotherapy, and hyperbaric oxygen. Br. J. Radiol., *56:* 251–255, 1983.
3. Kolstad, P. Intercapillary distance, oxygen tension, and local recurrence in cervix cancer. Scand. J. Clin. Lab. Invest. Suppl., *106:* 145–157, 1968.
4. Mueller-Klieser, W., Vaupel, P., Manz, R., and Schmidseder, R. Intracapillary oxyhemoglobin saturation of malignant tumors in humans. Int. J. Radiat. Oncol. Biol. Phys., *7:* 1397–1404, 1981.
5. Wendling, P., Menz, R., Thews, G., and Vaupel, P. Heterogeneous oxygenation of rectal carcinomas in humans. A critical parameter for preoperative irradiation. *In:* D. Bruley, H. I. Bicher, and D. Reneau (eds.), Oxygen Transport to Tissue, pp. 295–300. London: Plenum Publishing Corp., 1985.
6. Sutherland, R. M., Eddy, H. A., Bareham, B., Reich, K., and Vanantwerp, D. Resistance to Adriamycin in multicellular spheroids. Int. J. Radiat. Oncol. Biol. Phys., *5:* 1225–1230, 1979.
7. Kennedy, K. A., Teicher, B. A., Rockwell, S., and Sartorelli, A. C. The hypoxic tumor cell: a target for selective cancer chemotherapy. Biochem. Pharmacol., *29:* 1–8, 1980.
8. Jones, D. P. Hypoxia and drug metabolism. Biochem. Pharmacol., *30:* 1019–1023, 1981.
9. Sutherland, R. M., McCredie, J. A., and Inch, W. R. Growth of multicell spheroids in tissue culture as a model of nodular carcinomas. J. Natl. Cancer Inst., *46:* 113–120, 1971.
10. Sutherland, R. M., and Durand, R. E. Radiation response of multicell spheroids—an *in vitro* tumor model. Curr. Top. Radiat. Res., *11:* 87–139, 1976.
11. Acker, H., Carlsson, J., Durand, R., and Sutherland, R. M. (eds.). Spheroids in Cancer Research: Methods and Perspectives. Berlin: Springer Verlag, 1984.
12. Freyer, J. P., and Sutherland, R. M. Selective dissociation and characterization of cells from different regions of multicell tumor spheroids. Cancer Res., *40:* 3956–3965, 1980.
13. Bauer, K. D., Keng, P., and Sutherland, R. M. Isolation of quiescent cells from multicellular tumor spheroids using centrifugal elutriation. Cancer Res., *42:* 72–78, 1982.
14. Mueller-Klieser, W., and Sutherland, R. M. Influence of convection in the growth medium on oxygen tensions in multicellular tumor spheroids. Cancer Res., *42:* 237–242, 1982.
15. Mueller-Klieser, W., and Sutherland, R. M. Oxygen tensions in multicellular spheroids of two cell lines. Br. J. Cancer, *45:* 256–264, 1982.
16. Carlsson, J., Stalmacke, C. G., Acker, H., Haji-Karim, M., Nilsson, S., and Larsson, B. The influence of oxygen on viability and proliferation in cellular spheroids. Int. J. Radiat. Oncol. Biol. Phys., *5:* 2011–2020, 1979.
17. Durand, R. E., and Sutherland, R. M. Intercellular contact: its influence on the Dq of mammalian cell survival curves. *In:* T. Alper (ed.), Cell Survival after Low Doses of Radiation, Sixth L. H. Gray Conference, Bedford College, London, pp. 237–247. New York: Wiley, 1975.
18. Sacks, P. G., Miller, M. W., and Sutherland, R. M. Influences of growth conditions and cell-cell contact on responses of tumor cells to ultrasound. Radiat. Res., *87:* 175–186, 1981.
19. Durand, R. E. Effects of hyperthermia on the cycling, noncycling, and hypoxic cells of irradiation and unirradiated multicell spheroids. Radiat. Res., *75:* 373–384, 1978.

20. Dertinger, H., and Hulser, D. F. Intercellular communication in spheroids. *In:* H. Acker, J. Carlsson, R. Durand, and R. M. Sutherland (eds.), Spheroids in Cancer Research: Methods and Perspectives, pp. 67–83. Berlin: Springer-Verlag, 1984.
21. Olive, P., and Durand, R. Effect of intercellular contact on DNA conformation, radiation-induced DNA damage, and mutation in Chinese hamster V79 cells. Radiat. Res., *101:* 94–101, 1985.
22. Freyer, J. P., Tustanoff, E., Franko, A. J., and Sutherland, R. M. *In situ* oxygen consumption rates of cells in V-79 multicellular spheroids during growth. J. Cell. Physiol., *118:* 53–61, 1984.
23. Freyer, J. P., and Sutherland, R. M. A reduction in the *in situ* rates of oxygen and glucose consumption of cells in EMT6/Ro spheroids during growth. J. Cell. Physiol., *124:* 516–524, 1985.
24. Mueller-Kleiser, W., Bourrat, B., Gabbert, H., and Sutherland, R. M. Changes in O_2 consumption of multicellular spheroids during development of necrosis. Adv. Exp. Med. Biol., *191:* 775–784, 1985.
25. Mueller-Klieser, W., Freyer, J. P., and Sutherland, R. M. Influence of glucose and oxygen supply conditions on the oxygenation of multicellular spheroids. Br. J. Cancer, *53:* 345–353, 1986.
26. Landry, J., and Freyer, J. P. Regulatory mechanisms in spheroidal aggregates of normal and cancerous cells. *In:* H. Acker, J. Carlsson, R. Durand, and R. M. Sutherland (eds.), Spheroids in Cancer Research: Methods and Perspectives, pp. 50–66. Berlin: Springer-Verlag, 1984.
27. Steinberg, M. S. Reconstruction of tissues by dissociated cells. Science (Wash. DC), *141:* 401–408, 1963.
28. Schleich, A. Studies on aggregation of human ascites tumor cells. Eur. J. Cancer, *3:* 243–246, 1967.
29. Angello, J. C., and Hosick, H. L. Glycosaminoglycan synthesis by mammary tumor spheroids. Biochem. Biophys. Res. Commun., *107:* 1130–1137, 1982.
30. Nederman, T., Norling, B., Glimelius, B., Carlsson, J., and Brunk, V. Demonstration of an extracellular matrix in multicellular tumor spheroids. Cancer Res., *44:* 3090–3097, 1984.
31. Fogh, J., and Trempe, G. New human tumor cell lines. *In:* J. Fogh (ed.), Human Tumor Cells *in Vitro*, pp. 115–151. New York: Academic Press, 1975.
32. Lees, R. K., Sordat, B., and MacDonald, H. R. Multicellular tumor spheroids of human colon carcinoma origin: kinetic analysis of infiltration and *in situ* destruction in a xenogeneic (murine) host. Exp. Cell Biol., *49,* 207–219, 1981.
33. Barone, R. M., Calabro-Jones, P., Thomas, T. N., Sharp, T. R., and Byfield, J. E. Surgical adjuvant therapy in colon carcinoma: a human tumor spheroid model for evaluating radiation sensitizing agents. Cancer (Phila.), *47:* 2349–2357, 1981.
34. Mach, J.-P., Carrel, S., Merenda, C., Sordat, B., and Cerottini, J.-C. *In vivo* localization of radiolabelled antibodies to carcinoembryonic antigen in human colon carcinoma grafted into nude mice. Nature (Lond.), *248:* 704–709, 1984.
35. Franko, A. J., and Koch, C. J. The radiation response of hypoxia cells in EMT6 spheroids in suspension culture does model data from EMT6 tumours. Radiat. Res., *96:* 497–504, 1983.
36. Mueller-Klieser, W. Microelectrode measurement of oxygen tension distributions in multicellular spheroids cultured in spinner flasks. *In:* H. Acker, J. Carlsson, R. Durand, and R. M. Sutherland (eds.), Spheroids in Cancer Research: Methods and Perspectives, pp. 134–149. Berlin: Springer-Verlag, 1984.
37. Mueller-Klieser, W. Method for the determination of oxygen consumption rates and diffusion coefficients in multicellular spheroids. Biophys. J., *46:* 343–348, 1984.
38. Wang, W. R., Sordat, B., Piquet, D., and Sordat, M. Human colon tumors in nude mice: implantation site and expression of the invasive phenotype. *In:* B. Sordat (ed.), Immune-deficient Animals, pp. 239–245. Basel: Karger, 1984.
39. Schreyer, M., Haskell, C., Girardet, C., Buchegger, F., Carrel, S., and Mach, J.-P. Localisation of tumor-associated antigens on sections of human colon carcinoma grafted into nude mice with mouse monoclonal antibodies using the avidin-biotin-immunoperoxidase reaction. *In:* B. Sordat (ed.), Immune-deficient Animals, pp. 287–290. Basel: Karger, 1984.
40. Carlsson, J., and Acker, H. Influence of the oxygen pressure in the culture medium on the oxygenation of different types of multicellular spheroids. Int. J. Radiat. Oncol. Biol. Phys., *11:* 535–546, 1985.
41. Freyer, J. P. Role of necrosis in saturation of spheroid growth (abstract). Strahlentherapy, *160:* 58, 1984.